



Structural, elastic, electronic, and optical properties of NaAlSi₃O₈ and Al₄[Si₄O₁₀](OH)₈ from first-principles calculations

Ya-Le Tao¹ · Juan Gao¹ · Qi-Jun Liu¹ · Zheng-Tang Liu²

Received: 25 November 2022 / Accepted: 9 March 2023 / Published online: 25 March 2023
© The Author(s), under exclusive licence to Springer-Verlag GmbH Germany, part of Springer Nature 2023

Abstract

Context Based on the first-principles calculations, this paper investigates the structural, elastic, electronic, and optical properties of albite and kaolinite, respectively. It is determined that both of them show structural stability, mechanical stability, and brittleness by calculating formation enthalpy, phonon dispersion, elastic, and mechanically relevant properties. Both materials are insulators with an indirect bandgap. By calculating the TDOS and PDOS, the main characteristics of the electronic structure of NaAlSi₃O₈ come from O-2p and Si-3p states, O-2p, and Al-3p states hybridization, similar to Al₄[Si₄O₁₀](OH)₈. The covalence of Si–O bonds in NaAlSi₃O₈ is greater than Al–O bonds, and the covalent property sequence of Si–O bands in NaAlSi₃O₈ is Si2–O3 > Si1–O4 > Si2–O2 > Si1–O8 > Si1–O6 > Si3–O2 > Si3–O4. The optical anisotropy of NaAlSi₃O₈ and Al₄[Si₄O₁₀](OH)₈ is analyzed.

Methods First-principles density functional theory (DFT) calculation was carried out by the CASTEP computer program. The GGA-PW91 exchange–correlation was used. The energy convergence tolerance, the maximum force, and the maximum displacement were set in the calculation.

Keywords DFT · Albite · Kaolinite · Elastic properties · Optical properties

Introduction

Both albite and kaolinite are aluminosilicate with good insulating properties [1]. Albite can be used to make ceramics [2–6], glass [7, 8], tiles [9], catalysts [10], etc. Kaolinite can be used as a raw material for ceramics, paper making, catalysts [11–13], adsorbents [14–18], nanotube raw materials [19, 20], refractory materials [21], etc.

The physical and chemical properties of albite are now widely investigated. Liu et al. [22–24] investigated the thermodynamic stability of albite at high temperatures and pressures by means of molecular simulations. Li et al. [25] calculated isotopic fractionation coefficients for albite using

a reductive partitioning function. Factors responsible for the isotopic fractionation of silicon and oxygen in albite were investigated [26, 27]. Quantitative calculation of surface anisotropy of albite provided new ideas for selective grinding of aluminosilicate minerals based on crystal characteristics [28].

For kaolinite, the electronic structure of synthetic natural kaolinite was determined by combining X-ray absorption spectrum and first-principles calculation, and the band gap of synthetic kaolinite decreased with the formation of defects [29]. Based on DFT simulations to obtain the optical properties of kaolinite, the role of hydrogen bonding in the O–H bond has an impact on the photosynthesis of the crystal [30]. Weck et al. calculated the structural, mechanical, and thermodynamic properties of kaolinite using DFT-2. The calculated results are in good agreement with the experimental data [31]. The deformation and damage processes of kaolinite under tensile action were simulated by MD, with the tensile strength and Young's modulus decreasing with increasing temperature [32]. Studies on the adsorption principles of kaolinite were also being carried out, and the microscopic adsorption mechanisms of Ca(II) and K(I) on the surface of kaolinite were calculated using DFT [33]. The plane wave pseudopotential calculation was used to study the

✉ Juan Gao
gao.juan.xnjd@my.swjtu.edu.cn

✉ Qi-Jun Liu
qijunliu@home.swjtu.edu.cn

¹ Bond and Band Engineering Group, School of Physical Science and Technology, Southwest Jiaotong University, Chengdu 610031, People's Republic of China

² State Key Laboratory of Solidification Processing, Northwestern Polytechnical University, Xi'an 710072, People's Republic of China

adsorption of $[PbCl]^+$ by kaolinite on hydroxylated (001) substrate surface in aqueous system, and the mechanism of Pb–O (or Cl) bonding was discussed [34].

The computational simulations were accompanied by experimental measurements and calculations for both substances. By comparing the Raman spectra measured on naturally ordered and fully ordered albite with those calculated using WCILYD Hamiltonian quantities, it is demonstrated that the calculated vibrational wave numbers are in good agreement with those obtained from experimental measurements [35]. Cano et al. measured the optical absorption properties of albite by γ -rays, thermal resonance (EPR), and thermoluminescence (TL) and finally suggested the use of electron paramagnetism to understand the physical properties of albite [36]. The conductivity model of albite is proposed, which can clarify the conduction mechanism in a wide range of compositions and geological environments [37]. The elastic properties of albite are measured and compared with the simulation results [38, 39]. Liu et al. performed kinetic analysis of kaolinite decomposition at high temperature as well as the dehydroxylation reaction at 600 °C by TG-DSC [40]. Batch experiments were conducted to investigate the adsorption kinetics and equilibrium isotherm characteristics of vanadium (V) adsorption on natural kaolinite, and it was concluded that the adsorption kinetics on kaolinite was consistent with secondary kinetics, and the adsorption isotherm of vanadium (V) on kaolinite was more consistent with the Freundlich model [41]. However, a comprehensive study of the electronic, structural, elastic, and optical

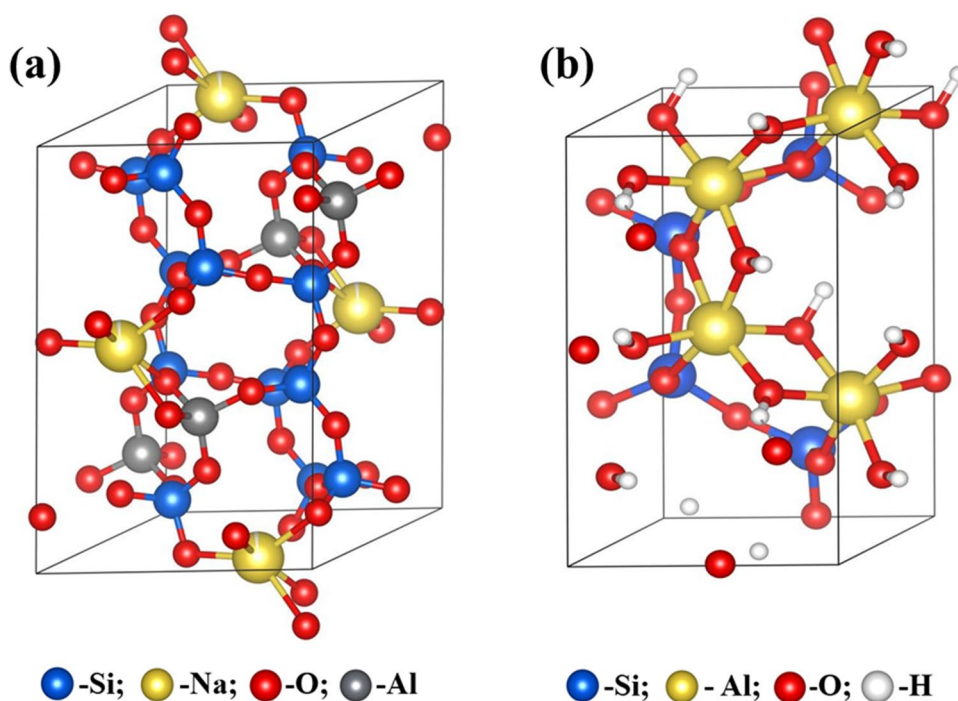
properties of albite and kaolinite has not been reported. In this paper, the electronic, structural, elastic, and optical properties of albite and kaolinite are analyzed computationally based on the first-principles calculations.

Computational details

The calculations for albite ($NaAlSi_3O_8$) and kaolinite ($Al_4[Si_4O_{10}](OH)_8$) were based on first-principles density functional theory (DFT) and were carried out by the CASTEP computer program [42]. The space group of $NaAlSi_3O_8$ is $P1$, and $Al_4[Si_4O_{10}](OH)_8$ is $P1$. And the crystal structure is triclinic, as shown in Fig. 1.

The calculated equilibrium lattice constants of $NaAlSi_3O_8$ are $a = 8.12 \text{ \AA}$, $b = 12.76 \text{ \AA}$, $c = 7.16 \text{ \AA}$; and of $Al_4[Si_4O_{10}](OH)_8$ are $a = 5.21 \text{ \AA}$, $b = 9.05 \text{ \AA}$, $c = 7.50 \text{ \AA}$. We used the GGA-PW91 functional to describe the exchange and correlation potential; the ultrasoft pseudopotential was used to describe electron-core interactions [43]. We set $5.0 \times 10^{-6} \text{ eV atom}^{-1}$ as the energy convergence tolerance, 0.01 eV \AA^{-1} as the maximum force, 0.02 GPa as the maximum stress, and $5.0 \times 10^{-4} \text{ \AA}$ as the maximum displacement. For $NaAlSi_3O_8$, we applied the Monkhorst–Pack grid to generate the 212 k-point grids [44]. We used the Na $2s^2 2p^6 3s^1$, O $2s^2 2p^4$, Al $3s^2 3p^1$, and Si $3s^2 3p^2$ as valence electrons. For $Al_4[Si_4O_{10}](OH)_8$, we applied the Monkhorst–Pack grid to generate the 322 k-point grids. We took the H $1s^1$, O $2s^2 2p^4$, Al $3s^2 3p^1$, and Si $3s^2 3p^2$ as valence electrons.

Fig. 1 Crystal structure of (a) $NaAlSi_3O_8$ and (b) $Al_4[Si_4O_{10}](OH)_8$. (The blue ball represents atom Si, the yellow ball represents atom Na, the red ball represents atom O, the gray ball represents atom Al, and the white ball represents atom H)



Results and discussion

Structural properties of NaAlSi₃O₈ and Al₄[Si₄O₁₀](OH)₈

Based on the first-principles study, we carry out geometric optimization calculation for crystal structure in within the GGA-PW91 functional. The atom coordinates of NaAlSi₃O₈ and Al₄[Si₄O₁₀](OH)₈ are shown in Tables 1 and 2 [45, 46]. The obtained lattice constants are organized in Table 3. By comparing the calculated results, it can be seen that the lattice constants calculated by us are consistent with the previous calculations and experimental results [45, 46]. Therefore, the calculation method of geometric optimization is reasonable.

Structural stability of NaAlSi₃O₈ and Al₄[Si₄O₁₀](OH)₈

It is necessary to predict the stability of structures before computing physical properties [47–51]. In order to predict the dynamic stability of materials, we calculated the phonon density of state and phonon dispersion of NaAlSi₃O₈ and Al₄[Si₄O₁₀](OH)₈.

The thermodynamic stability of the NaAlSi₃O₈ and Al₄[Si₄O₁₀](OH)₈ can be predicted by calculating the formation enthalpy (ΔH). It can be obtained by the following formula:

$$\Delta H(\text{NaAlSi}_3\text{O}_8) = \frac{1}{13} (E_{\text{total}}(\text{NaAlSi}_3\text{O}_8) - E_{\text{Na}} - E_{\text{Al}} - 3E_{\text{Si}} - 8E_{\text{O}}) \quad (1)$$

$$\Delta H(\text{Al}_4[\text{Si}_4\text{O}_{10}](\text{OH})_8) = \frac{1}{34} (E_{\text{total}}(\text{Al}_4[\text{Si}_4\text{O}_{10}](\text{OH})_8) - 4E_{\text{Al}} - 4E_{\text{Si}} - 18E_{\text{O}} - 8E_{\text{H}}) \quad (2)$$

Table 1 NaAlSi₃O₈ atom coordinates

Element	(This work)	Coordinates(x, y, z) (Expt. [45])
Na	(0.2633, 0.9905, 0.1434)	(0.2759, 0.9882, 0.1466)
Al	(0.0084, 0.1671, 0.2074)	(0.0094, 0.1727, 0.2102)
Si1	(0.0028, 0.8218, 0.2371)	(0.0051, 0.8198, 0.2372)
Si2	(0.6889, 0.1098, 0.3120)	(0.6974, 0.1124, 0.3221)
Si3	(0.6770, 0.8817, 0.3594)	(0.6886, 0.8826, 0.3605)
O1	(0.0063, 0.1279, 0.9661)	(0.0049, 0.1359, 0.9703)
O2	(0.5859, 0.9975, 0.2783)	(0.6038, 0.9993, 0.2841)
O3	(0.8111, 0.1069, 0.1882)	(0.8140, 0.1186, 0.1967)
O4	(0.8182, 0.8518, 0.2592)	(0.8233, 0.8520, 0.2555)
O5	(0.0077, 0.3016, 0.2674)	(0.0203, 0.3062, 0.2696)
O6	(0.0214, 0.6945, 0.2244)	(0.0275, 0.6940, 0.2413)
O7	(0.2115, 0.1088, 0.3890)	(0.2029, 0.1119, 0.3921)
O8	(0.1851, 0.8682, 0.4379)	(0.1808, 0.8694, 0.4301)

Table 2 Al₄[Si₄O₁₀](OH)₈ atom coordinates

Element	Coordinates(x, y, z) (This work)	Coordinates(x, y, z) (Expt. [46])
Si1	(0.0589, 0.3395, 0.0741)	(0.0678, 0.3494, 0.0564)
Si2	(0.0734, 0.6679, 0.0756)	(0.0837, 0.6504, 0.0865)
Si3	(0.5595, 0.8394, 0.0742)	(0.5437, 0.8414, 0.0765)
Si4	(0.5731, 0.1679, 0.0756)	(0.5618, 0.1813, 0.0675)
Al1	(0.3594, 0.4912, 0.4577)	(0.3541, 0.5055, 0.4706)
Al2	(0.3525, 0.8272, 0.4554)	(0.3738, 0.8295, 0.4516)
Al3	(0.8600, 0.9913, 0.4578)	(0.8761, 0.9975, 0.4706)
Al4	(0.8520, 0.3272, 0.4553)	(0.8489, 0.3315, 0.4606)
H1	(0.2035, 0.0602, 0.3049)	(0.2448, 0.0724, 0.3445)
H2	(0.1210, 0.1670, 0.7106)	(0.1738, 0.1874, 0.7136)
H3	(0.1022, 0.5008, 0.7087)	(0.0738, 0.5264, 0.7055)
H4	(0.1099, 0.8147, 0.7116)	(0.0838, 0.8384, 0.7155)
H5	(0.7030, 0.5603, 0.3053)	(0.6918, 0.5524, 0.2525)
H6	(0.6219, 0.6669, 0.7102)	(0.6238, 0.6474, 0.7206)
H7	(0.6033, 1.0001, 0.7092)	(0.5938, 0.9824, 0.7226)
H8	(0.6086, 0.3141, 0.7111)	(0.6067, 0.2954, 0.7045)
O1	(0.1107, 0.3528, 0.2952)	(0.1100, 0.3420, 0.3070)
O2	(0.1830, 0.6618, 0.2963)	(0.1487, 0.6614, 0.2905)
O3	(0.0567, 0.5017, 0.9821)	(0.0827, 0.4884, 0.9734)
O4	(0.2753, 0.2364, 1.0064)	(0.2596, 0.2203, 0.9804)
O5	(0.2693, 0.7634, 0.9827)	(0.2347, 0.7683, 0.9654)
O6	(0.6113, 0.8527, 0.2953)	(0.6269, 0.8435, 0.2945)
O7	(0.6830, 0.1618, 0.2963)	(0.6857, 0.1574, 0.3075)
O8	(0.5569, 0.0017, 0.9822)	(0.5487, 0.0033, 0.9764)
O9	(0.7759, 0.7366, 0.0063)	(0.7716, 0.7253, 0.0304)
O10	(0.7687, 0.2635, 0.9825)	(0.7667, 0.2624, 0.9824)
O11	(0.1108, 0.9668, 0.3077)	(0.1177, 0.9674, 0.3125)
O12	(0.0135, 0.1626, 0.5834)	(0.0247, 0.1724, 0.5845)
O13	(0.0979, 0.4666, 0.5836)	(0.1287, 0.4654, 0.5854)
O14	(0.0995, 0.8548, 0.5903)	(0.1066, 0.8434, 0.5994)
O15	(0.6103, 0.4668, 0.3077)	(0.6077, 0.4683, 0.3044)
O16	(0.5138, 0.6624, 0.5833)	(0.5247, 0.6604, 0.5915)
O17	(0.5986, 0.9664, 0.5838)	(0.5936, 0.9744, 0.5774)
O18	(0.5987, 0.3546, 0.5900)	(0.5827, 0.3693, 0.5855)

where $E_{\text{total}}(\text{NaAlSi}_3\text{O}_8)$, $E_{\text{total}}(\text{Al}_4[\text{Si}_4\text{O}_{10}](\text{OH})_8)$, E_{Na} , E_{Al} , E_{Si} , E_{O} , and E_{H} are the calculated total energy of NaAlSi₃O₈, Al₄[Si₄O₁₀](OH)₈, Na, Al, Si, O, and H respectively.

The formation enthalpy, lattice parameters, and volume of the two materials are calculated as shown in Table 3. The results of the enthalpy of formation calculations show that both NaAlSi₃O₈ and Al₄[Si₄O₁₀](OH)₈ are thermodynamically stable, because the calculated formation enthalpy is less than zero.

The dynamical stability of materials is considered by the phonon dispersion and phonon density of state. No imaginary phonon frequency indicates that the material is dynamically stable. We calculated the phonon dispersion

Table 3 The calculated lattice parameters (a , b , c in Å, α , β , γ in °), formation enthalpy ΔH (in eV/atom), and volume (in Å³) of triclinic NaAlSi₃O₈ and Al₄[Si₄O₁₀](OH)₈ alloys

	a	b	c	α	β	γ	V	ΔH	References
NaAlSi ₃ O ₈	8.12	12.76	7.16	94.22	116.8	87.71	659.8	-2.24	This work
	8.15	12.78	7.16	94.28	116.7	87.74	665.4	—	Expt. [45]
Al ₄ [Si ₄ O ₁₀](OH) ₈	5.21	9.05	7.50	91.30	104.8	89.77	341.5	-1.65	This work
	5.15	8.93	7.38	91.93	105.0	89.79	—	—	Expt. [46]

and phonon density of state of NaAlSi₃O₈ and Al₄[Si₄O₁₀](OH)₈ separately, and the results are shown in Fig. 2. The results of Fig. 2 show that both materials have no phonon imaginary frequency. This indicates that they are both dynamically stable.

Elastic and mechanical properties of NaAlSi₃O₈ and Al₄[Si₄O₁₀](OH)₈

Mechanical stability is an important property when studying materials [52]. We use the elastic constant to describe the mechanical stability of a material and calculate it based on the linear stress–strain relationship equation $\sigma_{ij} = C_{ijkl}\epsilon_{kl}$. The number of elastic constants is inversely proportional to the symmetry of the compound. For triclinic NaAlSi₃O₈ and

Fig. 2 Calculated phonon dispersion and phonon density of state. (a) NaAlSi₃O₈. (b) Al₄[Si₄O₁₀](OH)₈

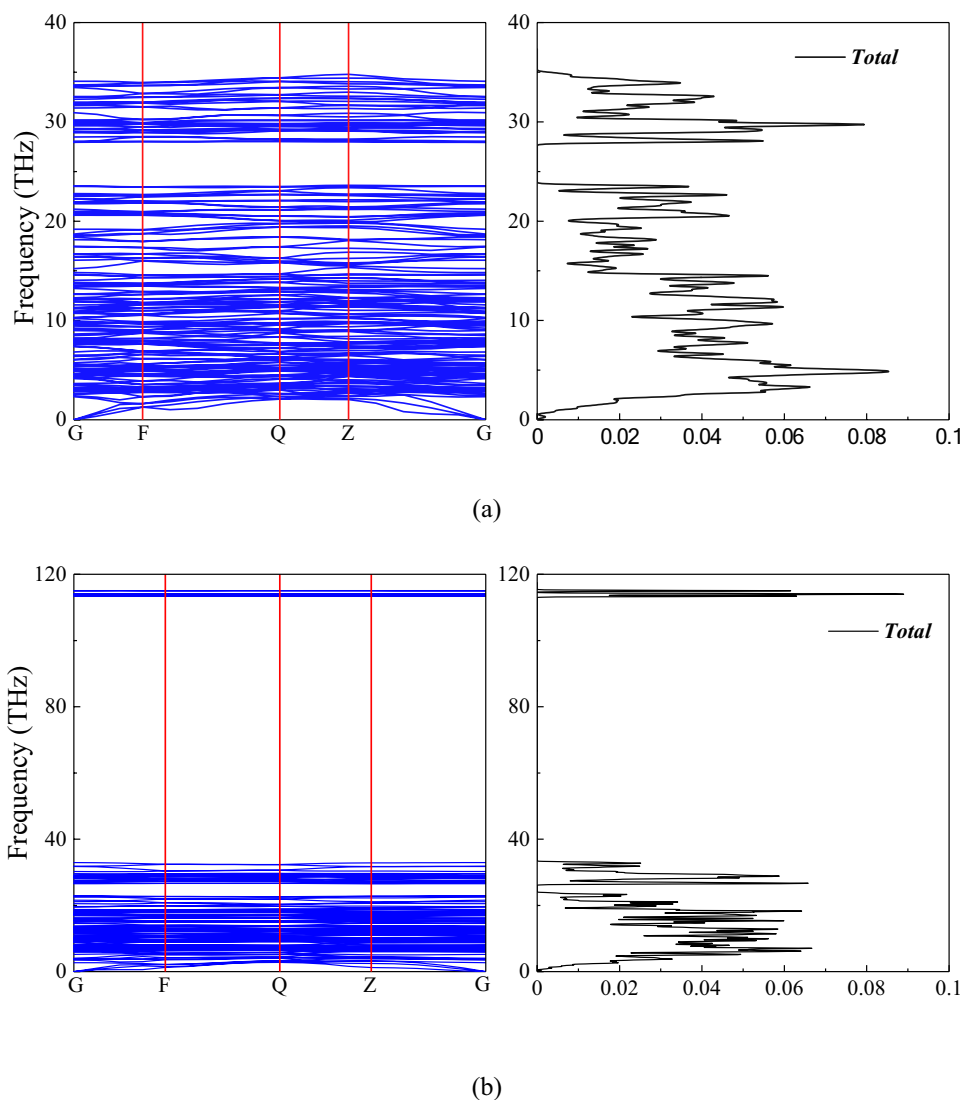


Table 4 Calculated elastic constants of triclinic NaAlSi₃O₈ and Al₄[Si₄O₁₀](OH)₈

	C ₁₁	C ₁₂	C ₁₃	C ₁₄	C ₁₅	C ₁₆	C ₂₂	C ₂₃
NaAlSi ₃ O ₈	73.69	32.06	40.00	0.04	−9.94	−4.09	178.91	24.58
	C ₂₄	C ₂₅	C ₂₆	C ₃₃	C ₃₄	C ₃₅	C ₃₆	C ₄₄
	−9.86	−6.67	−1.66	185.86	2.07	0.72	−2.99	32.80
	C ₄₅	C ₄₆	C ₅₅	C ₅₆	C ₆₆			
	−1.03	1.33	41.59	−0.01	49.76			
Al ₄ [Si ₄ O ₁₀](OH) ₈	C ₁₁	C ₁₂	C ₁₃	C ₁₄	C ₁₅	C ₁₆	C ₂₂	C ₂₃
	193.41	74.84	8.68	3.42	−36.62	−2.95	198.14	2.51
	C ₂₄	C ₂₅	C ₂₆	C ₃₃	C ₃₄	C ₃₅	C ₃₆	C ₄₄
	0.50	−19.57	−1.07	72.54	−0.24	−3.53	0.63	36.13
	C ₄₅	C ₄₆	C ₅₅	C ₅₆	C ₆₆			
	−2.21	−8.87	28.04	1.74	61.55			

Table 5 The bulk modulus B (GPa), shear modulus G (GPa), B/G , Young's modulus (E) (GPa), and Poisson's ratio (ν) of triclinic NaAlSi₃O₈ and Al₄[Si₄O₁₀](OH)₈

	B	G	B/G	E	ν
NaAlSi ₃ O ₈	64.26	44.02	1.46	107.50	0.22
Al ₄ [Si ₄ O ₁₀](OH) ₈	57.32	43.91	1.31	104.94	0.19

Al₄[Si₄O₁₀](OH)₈ crystal structure, there are 21 twenty-one independent elastic coefficients, as shown in Table 4.

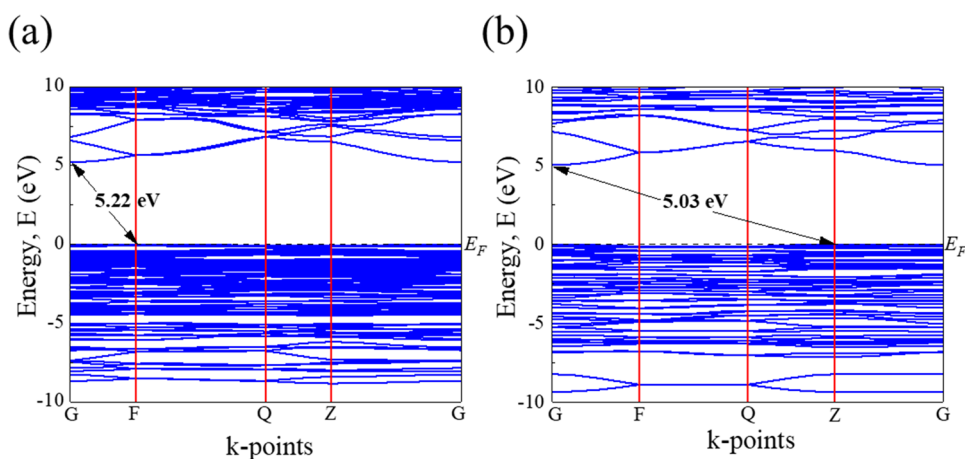
According to Born's [53] stability criterion and Eq. (12) in the paper written by Gao [54] et al., we know the stability criterion of the triclinic system. Both NaAlSi₃O₈ and Al₄[Si₄O₁₀](OH)₈ are mechanically stable structures. Based on the Voigt–Reuss–Hill approximation [55], we can use the elastic constants to obtain mechanical properties. This research calculates the bulk modulus (B), shear modulus (G), B/G , Young's modulus (E), and Poisson's ratio (ν) of NaAlSi₃O₈ and Al₄[Si₄O₁₀](OH)₈ respectively. The calculation formulas of Young's modulus and Poisson's ratio are:

$E = \frac{9BG}{3B+G}$ and $\nu = \frac{3B-2G}{6B+2G}$. The results of the calculations are shown in Table 5.

According to the data in Table 5, triclinic NaAlSi₃O₈ has greater resistance to volume deformation than Al₄[Si₄O₁₀](OH)₈. Brittleness/toughness is also the focus of material performance research. We can simply judge the brittleness/toughness of materials through B/G and Poisson's ratio. If B/G is greater than 1.75 [56], the material shows toughness; otherwise, it shows brittleness. Both NaAlSi₃O₈ and Al₄[Si₄O₁₀](OH)₈ are brittle. The order of brittleness is: Al₄[Si₄O₁₀](OH)₈ > NaAlSi₃O₈.

Electronic properties of NaAlSi₃O₈ and Al₄[Si₄O₁₀](OH)₈

As shown in the calculation results of energy band structure in Fig. 3, the black dashed line shows the Fermi energy level (E_F). Both triclinic NaAlSi₃O₈ and Al₄[Si₄O₁₀](OH)₈ are insulators with an indirect bandgap of 5.22 eV and 5.03 eV, respectively.

Fig. 3 Calculated band structure of (a) NaAlSi₃O₈ and (b) Al₄[Si₄O₁₀](OH)₈

The total density of states (TDOS) and partial density of states (PDOS) of $\text{NaAlSi}_3\text{O}_8$ and $\text{Al}_4[\text{Si}_4\text{O}_{10}](\text{OH})_8$ are calculated based on DFT, as shown in Figs. 4 and 5.

For $\text{NaAlSi}_3\text{O}_8$, the partial density of states of different Al, Si, O atoms are shown in Fig. 4, but they have different peaks. The formation of covalent bonds between these different Al, Si, O atoms is revealed. The main features of electronic structure mainly come from O-2p (including: O1-2p, O2-2p, O3-2p, O4-2p, O5-2p, O6-2p, O7-2p, O8-2p) and Si-3p (including: Si1-3p, Si2-3p, Si3-3p) states, O-2p and Al-3p states hybridization. The lowest energy states are from Na-2 s states. States from -22.5 to -15.0 eV are mainly due to O1-2 s, O2-2 s, O3-2 s, O4-2 s, O5-2 s, O6-2 s, O7-2 s, O8-2 s, and Na-2p states along with a small amount of Al-3 s, Al-3p, Si1-3 s, Si1-3p, Si2-3 s, Si2-3p, Si3-3 s, and Si3-3p states. And then, the upper valence bands (VBs) are mainly derived from O-2p and Si-3p states, O-2p and Al-3p states hybridization. For $\text{Al}_4[\text{Si}_4\text{O}_{10}](\text{OH})_8$,

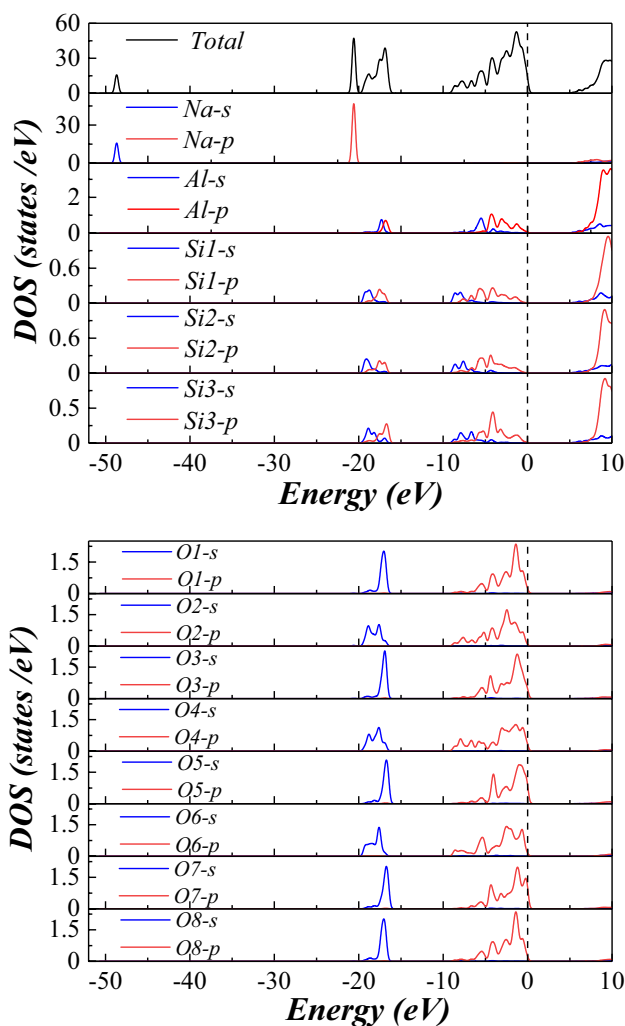


Fig. 4 The calculated TDOS and PDOS of $\text{NaAlSi}_3\text{O}_8$

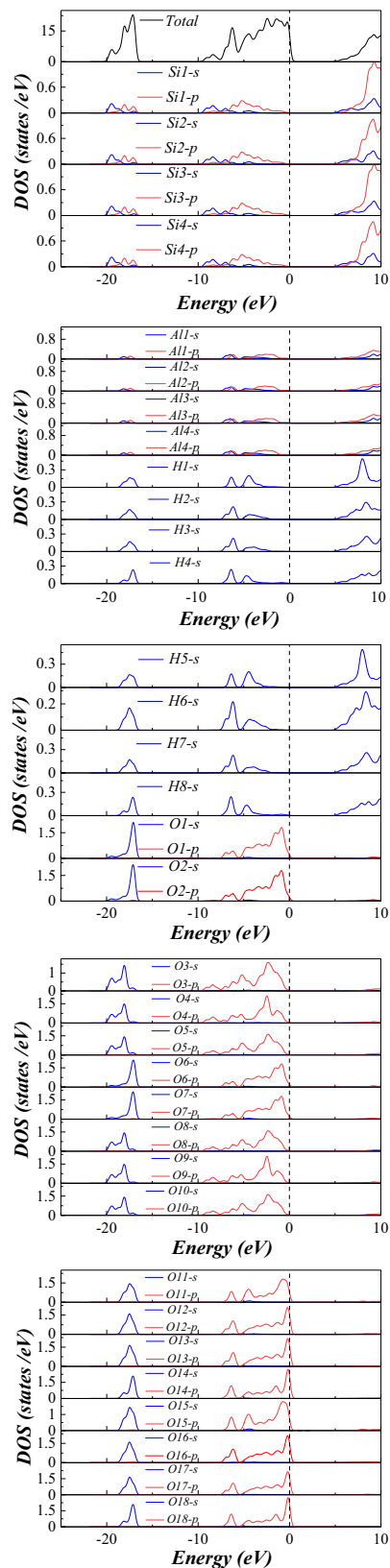


Fig. 5 The calculated TDOS and PDOS of $\text{Al}_4[\text{Si}_4\text{O}_{10}](\text{OH})_8$

the partial density of states for different Al, Si, O atoms are shown in Fig. 5, indicating the formation of covalent bonds between different Al, Si, O atoms. The main features of electronic structure are mainly due to O-2p (including: O1-2p, O2-2p, O3-2p, O4-2p, O5-2p, O6-2p, O7-2p, O8-2p, O9-2p, O10-2p, O11-2p, O12-2p, O13-2p, O14-2p, O15-2p, O16-2p, O17-2p, O18-2p) and Si-3p (including: Si1-3p, Si2-3p, Si3-3p, Si4-3p) states, O-2p and Al-3p (including: Al1-3p, Al2-3p, Al3-3p, Al4-3p) states hybridization. Then, the upper valence bands (VBs) come from nonbonding O1-2p, O2-2p, O6-2p, O7-2p, O11-2p, and O15-2p states.

Tables 6 and 7 show the calculated Mulliken charges, bond lengths, and bond populations of triclinic NaAlSi₃O₈ and Al₄[Si₄O₁₀](OH)₈.

Positive or negative Mulliken charge means gaining or losing electrons. For NaAlSi₃O₈, Na, Al, and Si are all transferring charge while O is gaining charge. Si–O and Al–O bonds are mainly form covalent bonds and a small amount of ionic bonds, and Si is more capable of losing electrons than Al. Therefore, the covalence of Si–O bonds is greater than Al–O bonds. The ionic and covalent properties of atomic bonding can be directly characterized by the bond population. When the bond population value is positive/negative, it represents bonding/nonbonding. With the increase of the bond population, the covalent properties of bonding between atoms become stronger. As shown in Table 6, the Si–O bonds have the strongest covalency and are not easily broken. The order of covalency of Si–O bands is Si2–O3 > Si1–O4 > Si2–O2 > Si1–O8 > Si1–O6 > Si3–O2 > Si3–O4. Na–O bonds have the smallest bond population, which is mainly reflected in ionic property.

For Al₄[Si₄O₁₀](OH)₈, the individual atomic Mulliken charges are shown in Table 7. Si, Al, and H are all transfer charge, while O gains charge. The Si–O bonds and Al–O bonds are mainly covalent bonds. And O–H bonds form hydrogen bonds, which are much less powerful than chemical bonds. According to the calculation of bond populations and bond lengths, the bond populations of Si–O bonds are obviously larger than Al–O bonds, and bond lengths of Si–O bonds are smaller than Al–O bonds. Therefore, the covalence of Si–O bonds is greater than Al–O bonds. By comparing the different Si–O bonds, the Si1–O1 bond populations is the largest among different bonds. Compared with the Al–O bands, Al1–O18 bonds have the largest bond populations. In addition, both Al–O and Si–O bonds are covalent bonds. And the order of strength of the covalent bonding action is Si1–O1 > Si1–O4 > Si1–O3 > Si1–O10 > Al1–O18 > Al1–O13 > Al1–O16 > Al1–O1 > Al1–O15 > Al1–O2.

Charge density difference is also an important method to study the electronic structure, which can visualize the electron flow and bonding properties. We calculated the electron density difference for the NaAlSi₃O₈ along the (001) plane and Al₄[Si₄O₁₀](OH)₈ along the (010) plane as shown in Fig. 6.

It can be seen from Fig. 6(a) that Si and Al atoms in NaAlSi₃O₈ form covalent bonds with O atoms respectively, where both Si and Al atoms lose electrons and O atoms get electrons. It can be clearly seen that the ability of Si atom to lose electrons is greater than that of Al atom, and the covalence of Si–O bonds is greater than that of Al–O bonds. Similarly, it can be seen from Fig. 6(b) that both Si and Al atoms in Al₄[Si₄O₁₀](OH)₈ lose electrons, and O atoms gain electrons, and the covalence of Si–O bonds is greater than that of Al–O bonds.

Table 6 Calculated Mulliken charges (*e*), bond lengths (Å), and bond populations (*e*) of NaAlSi₃O₈

Species	<i>s</i>	<i>p</i>	<i>d</i>	Total	Charge [<i>e</i>]	Bonds	Bond populations (<i>e</i>)	Bond lengths (Å)
Na	2.04	5.78	0	7.82	1.18	Si1–O4	0.58	1.60
Al	0.44	0.76	0	1.2	1.8	Si1–O6	0.54	1.62
Si1	0.61	1.21	0	1.82	2.18	Si1–O8	0.56	1.62
Si2	0.63	1.23	0	1.86	2.14	Si2–O2	0.57	1.63
Si3	0.64	1.27	0	1.91	2.09	Si2–O3	0.64	1.60
O1	1.85	5.36	0	7.21	−1.21	Si3–O2	0.53	1.65
O2	1.84	5.32	0	7.16	−1.16	Si3–O4	0.52	1.62
O3	1.85	5.33	0	7.18	−1.18	Al–O1	0.45	1.76
O4	1.81	5.36	0	7.17	−1.17	Al–O3	0.46	1.75
O5	1.86	5.31	0	7.17	−1.17	Al–O5	0.46	1.74
O6	1.83	5.32	0	7.15	−1.15	Al–O7	0.45	1.75
O7	1.85	5.32	0	7.17	−1.17	Na–O2	0.01	2.35
O8	1.82	5.34	0	7.16	−1.16	Na–O7	0.07	2.40

Table 7 Calculated Mulliken charges (e), bond lengths (\AA), and bond populations (e) of $\text{Al}_4[\text{Si}_4\text{O}_{10}](\text{OH})_8$

Species	s	p	d	Total	Charge [e]	Bonds	Bond populations (e)	Bond lengths (\AA)
Al1	0.46	0.7	0	1.16	1.84	Si1-O1	0.63	1.611
Al2	0.46	0.7	0	1.16	1.84	Si1-O3	0.52	1.634
Al3	0.46	0.7	0	1.16	1.84	Si1-O4	0.52	1.631
Al4	0.46	0.7	0	1.16	1.84	Si1-O10	0.52	1.639
Si1	0.61	1.15	0	1.75	2.25	Al1-O1	0.28	1.967
Si2	0.61	1.15	0	1.76	2.24	Al1-O2	0.24	2.048
Si3	0.61	1.15	0	1.75	2.25	Al1-O13	0.31	1.861
Si4	0.61	1.15	0	1.76	2.24	Al1-O15	0.27	1.938
O1	1.85	5.28	0	7.13	-1.13	Al1-O16	0.31	1.868
O2	1.85	5.28	0	7.13	-1.13	Al1-O18	0.33	1.865
O3	1.84	5.31	0	7.15	-1.15	H1-O1	0.00	2.689
O4	1.83	5.33	0	7.16	-1.16	H1-O7	-0.00	2.682
O5	1.84	5.31	0	7.15	-1.15	H1-O11	0.61	0.979
O6	1.85	5.28	0	7.13	-1.13	H1-O12	-0.01	2.675
O7	1.85	5.28	0	7.13	-1.13	H1-O17	-0.01	2.683
O8	1.84	5.31	0	7.15	-1.15			
O9	1.83	5.33	0	7.16	-1.16			
O10	1.84	5.31	0	7.15	-1.15			
O11	1.85	5.18	0	7.04	-1.04			
O12	1.83	5.23	0	7.07	-1.07			
O13	1.83	5.24	0	7.07	-1.07			
O14	1.83	5.24	0	7.07	-1.07			
O15	1.85	5.18	0	7.04	-1.04			
O16	1.83	5.23	0	7.07	-1.07			
O17	1.83	5.24	0	7.07	-1.07			
O18	1.83	5.24	0	7.07	-1.07			
H1	0.57	0	0	0.57	0.43			
H2	0.55	0	0	0.55	0.45			
H3	0.55	0	0	0.55	0.45			
H4	0.55	0	0	0.55	0.45			
H5	0.57	0	0	0.57	0.43			
H6	0.55	0	0	0.55	0.45			
H7	0.55	0	0	0.55	0.45			
H8	0.55	0	0	0.55	0.45			

Optical properties of $\text{NaAlSi}_3\text{O}_8$ and $\text{Al}_4[\text{Si}_4\text{O}_{10}](\text{OH})_8$

The optical properties resulting from the electronic transition can be calculated by the first-principles. First, dispersion of optical functions can be expressed as [57]: $\varepsilon(\omega) = \varepsilon_1(\omega) + i\varepsilon_2(\omega)$. The imaginary part $\varepsilon_2(\omega)$ is related to electronic transition, and the expression formula is shown below:

$$\varepsilon_2(\omega) = \frac{4\pi^2}{m^2\omega^2} \sum_{i,j} \int \langle i|M|j \rangle^2 f_i(1-f_j) \times \delta(E_f - E_i - \omega) d^3k \quad (3)$$

(Eq. M – dipole matrix; i – initial states; j – final states; f_i – the Fermi distribution function for the i th state; E_i – energy of electron in the i th state)

According to the Kramers–Kronig dispersion relation system [58], the real part $\varepsilon_1(\omega)$ can be expressed as [59, 60]:

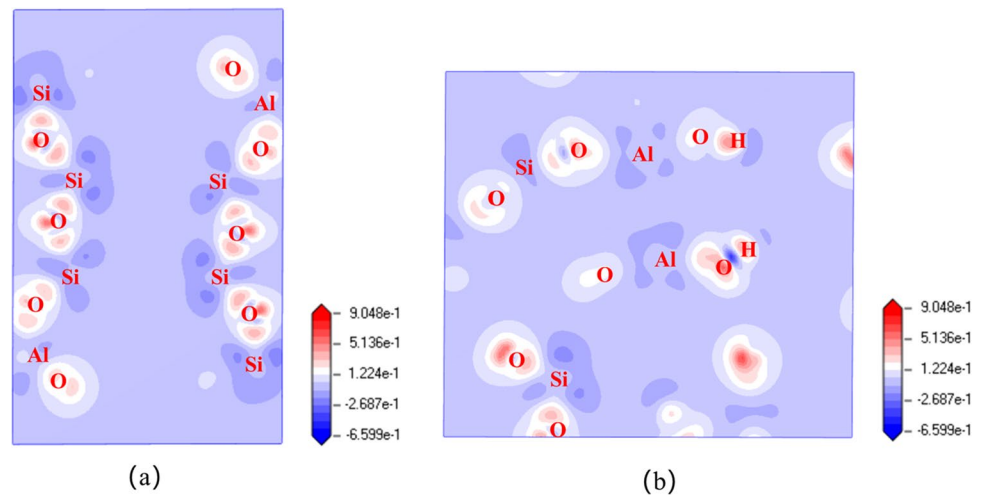
$$\varepsilon_1(\omega) = 1 + \frac{2}{\pi} Q \int_0^\infty \frac{\omega'^2 \varepsilon_2(\omega') d\omega'}{(\omega'^2 - \omega^2)} \quad (4)$$

$$P = \lim_{a \rightarrow 0} \int_{-\infty}^{\omega-a} \frac{\varepsilon(\omega')}{\omega' - \omega} d\omega' + \lim_{a \rightarrow 0} \int_{\omega+a}^{+\infty} \frac{\varepsilon(\omega')}{\omega' - \omega} d\omega' \quad (5)$$

(Eq. Q – principal value of the integral)

From the above formula, it can be deduced that the material's refractive index $n(\omega)$, extinction coefficient $k(\omega)$,

Fig. 6 Calculated charge density difference of (a) $\text{NaAlSi}_3\text{O}_8$ (along the (001) plane) and (b) $\text{Al}_4[\text{Si}_4\text{O}_{10}](\text{OH})_8$ (along the (010) plane)



reflectivity $R(\omega)$, absorption coefficient $I(\omega)$, loss function $L(\omega)$, and optical conductivity $\sigma(\omega)$. The specific relationship is as follows:

$$n(\omega) = \left[\frac{\varepsilon_1(\omega) + \sqrt{\varepsilon_1(\omega)^2 + \varepsilon_2(\omega)^2}}{2} \right]^{1/2} \quad (6)$$

$$k(\omega) = \left[\frac{-\varepsilon_1(\omega) + \sqrt{\varepsilon_1(\omega)^2 + \varepsilon_2(\omega)^2}}{2} \right]^{1/2} \quad (7)$$

$$R(\omega) = \left| \frac{\varepsilon^{1/2}(\omega) - 1}{\varepsilon^{1/2}(\omega) + 1} \right|^2 \quad (8)$$

$$I(\omega) = \sqrt{2}(\omega) \left(\sqrt{\varepsilon_1(\omega)^2 + \varepsilon_2(\omega)^2} - \varepsilon_1(\omega) \right)^{1/2} \quad (9)$$

$$L(\omega) = -\text{Im} \left(\frac{1}{\varepsilon(\omega)} \right) = \frac{\varepsilon_2(\omega)}{\varepsilon_1^2(\omega) + \varepsilon_2^2(\omega)} \quad (10)$$

$$\sigma(\omega) = \sigma_1(\omega) + i\sigma_2(\omega) = -i \frac{\omega}{4\pi} [\varepsilon(\omega) - 1] \quad (11)$$

The calculated dielectric functions are shown in Fig. 7.

It can be seen that $\text{NaAlSi}_3\text{O}_8$ and $\text{Al}_4[\text{Si}_4\text{O}_{10}](\text{OH})_8$ have different optical anisotropy. For $\text{NaAlSi}_3\text{O}_8$, imaginary part $\varepsilon_2(\omega)$ depends on the transition of valence band electrons and conduction band electrons. We can see that the imaginary part $\varepsilon_2(\omega)$ shows two peaks which mainly come from the electron transition of Si1-3p, Si2-3p, Si3-3p, and Al-3p states. The first peak position appears near

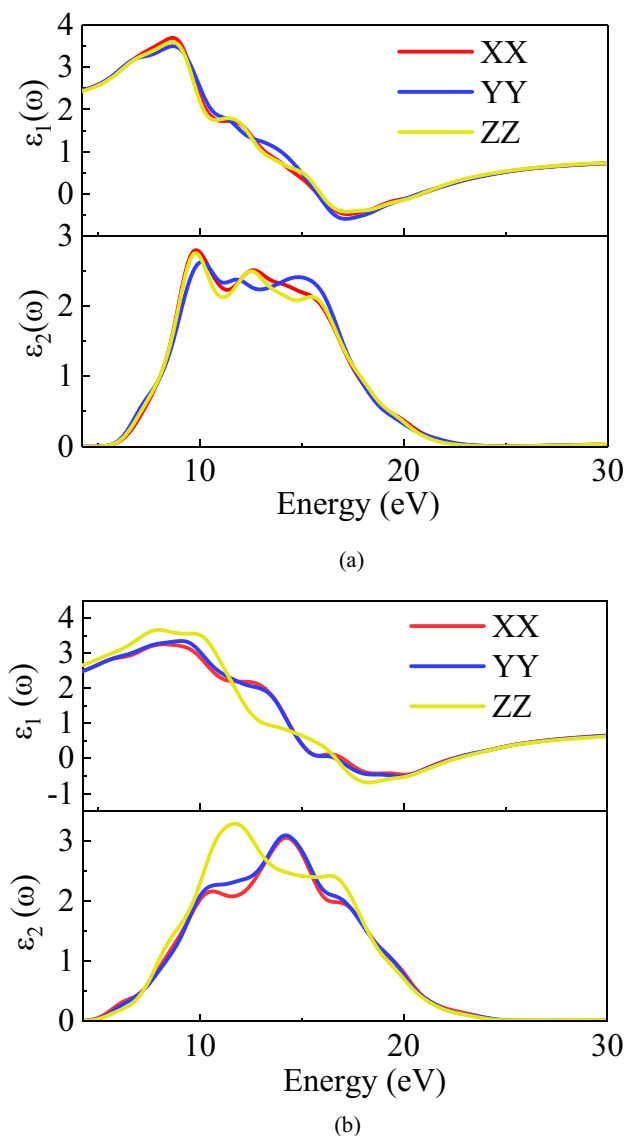
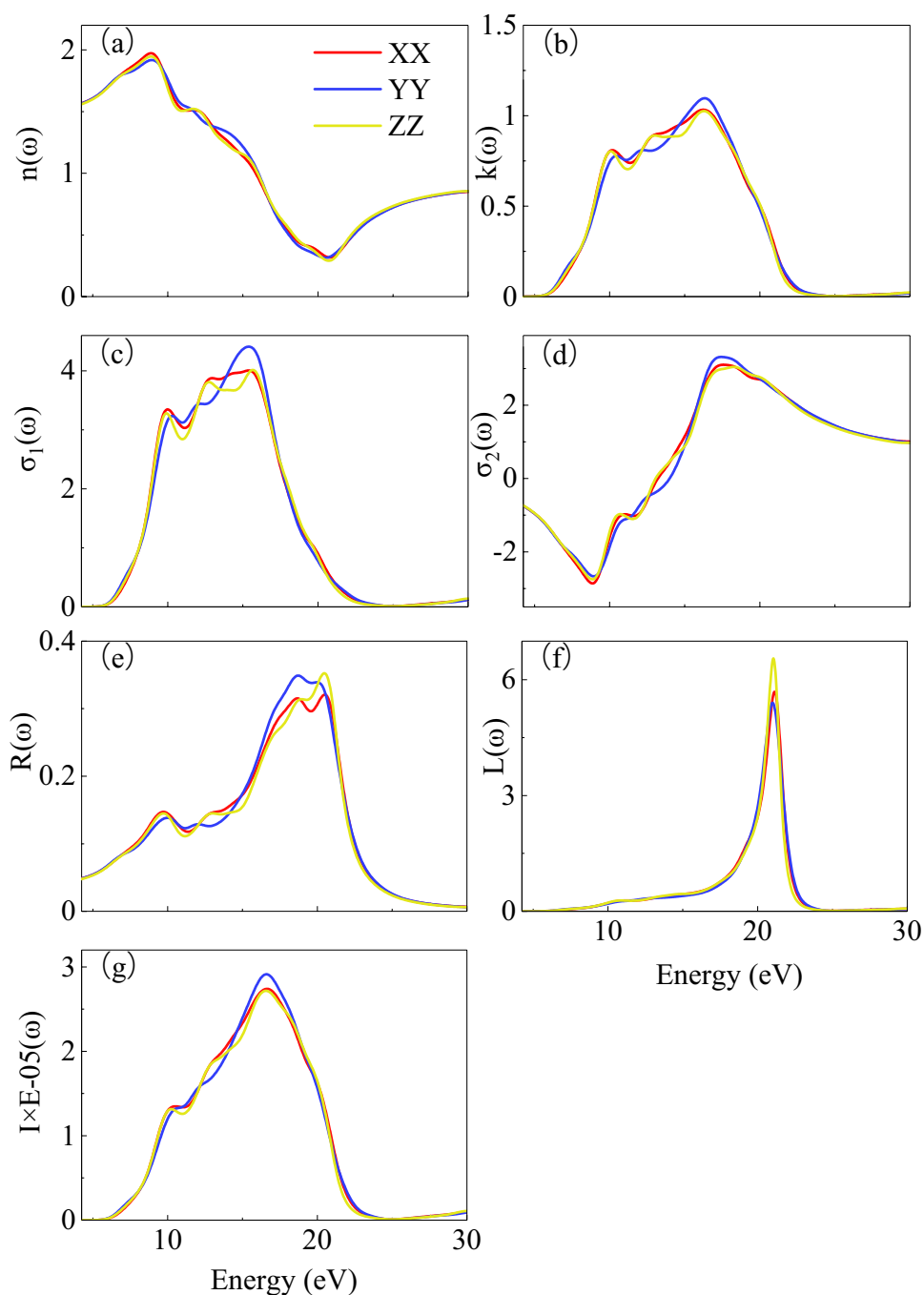


Fig. 7 The calculated imaginary part $\varepsilon_2(\omega)$ and real part $\varepsilon_1(\omega)$ of the dielectric function $\varepsilon(\omega)$ of (a) $\text{NaAlSi}_3\text{O}_8$ and (b) $\text{Al}_4[\text{Si}_4\text{O}_{10}](\text{OH})_8$

Fig. 8 The calculated (a) refractive index $n(\omega)$; (b) refractive index $k(\omega)$; (c) optical conductivity $\sigma_1(\omega)$; (d) optical conductivity $\sigma_2(\omega)$; (e) reflectivity $R(\omega)$; (f) loss function $L(\omega)$; and (g) absorption coefficient $I(\omega)$ of $\text{NaAlSi}_3\text{O}_8$

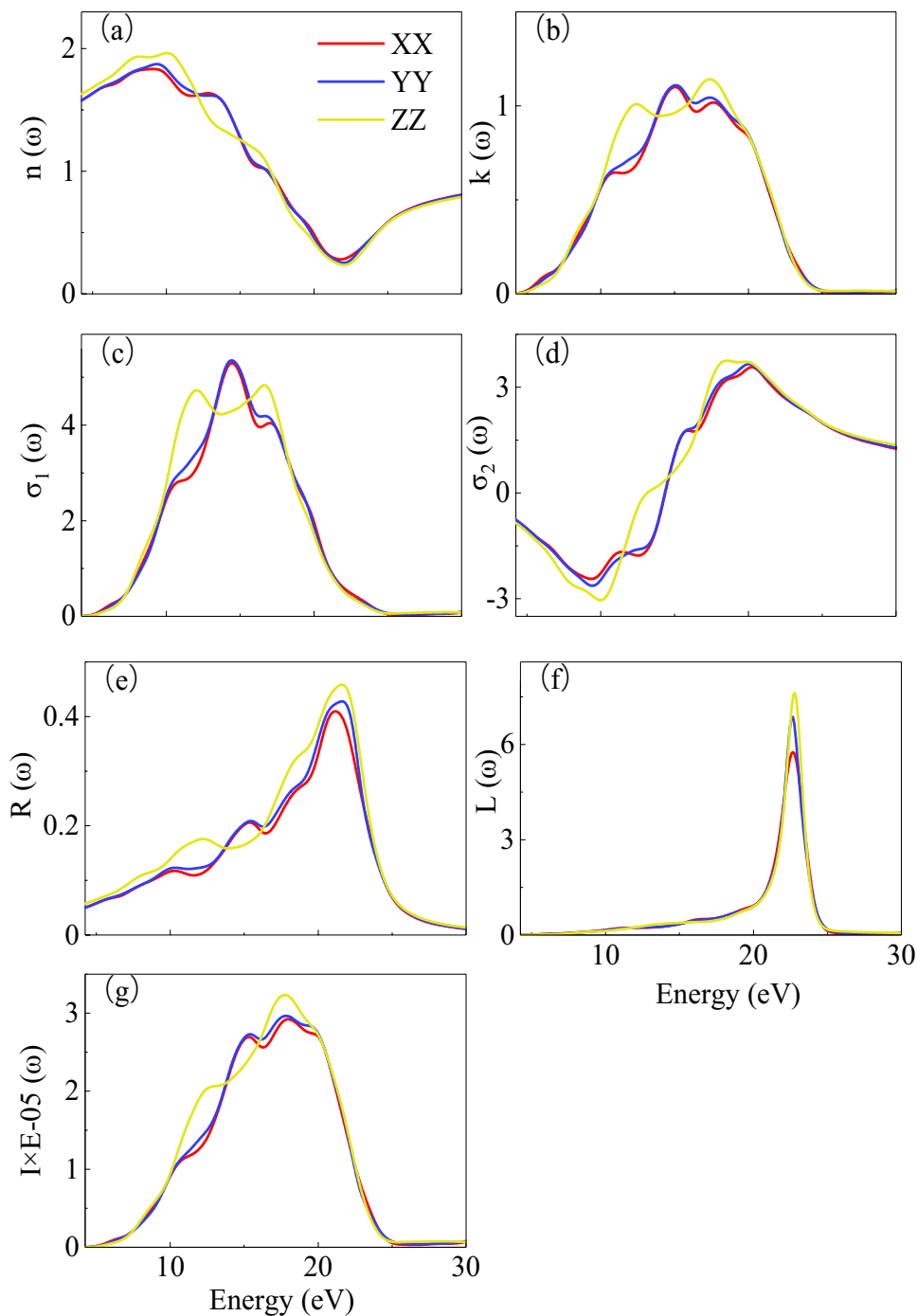


10 eV, similar to real part $\epsilon_1(\omega)$. With regard to $\text{Al}_4[\text{Si}_4\text{O}_{10}](\text{OH})_8$, there are three peaks present in the $\epsilon_2(\omega)$, it mainly comes from the electron transition of O-2p states and the hybridization between O-2p and Si-3p states, O-2p, and Al-3p states. Specially, the peak of the dielectric imaginary part in the z direction moves towards the low-energy region and increases in peak value.

The calculated values of absorption coefficient, reflectivity, optical conductivity, and loss function of $\text{NaAlSi}_3\text{O}_8$ and $\text{Al}_4[\text{Si}_4\text{O}_{10}](\text{OH})_8$ are shown in Figs. 8 and 9.

It can be seen from Fig. 8 that the tendency of the refractive index $n(\omega)$ of $\text{NaAlSi}_3\text{O}_8$ corresponds to the real part $\epsilon_1(\omega)$ of the dielectric function. The refractive index fluctuates widely in the energy range from 10 to 20 eV. It rises slowly from 20 to 30 eV. The extinction coefficient $k(\omega)$ achieves a maximum value at the energy of 16.3 eV. And the absorption coefficient is the proportion of energy attenuation of a light wave per unit distance through a semiconductor medium. $\text{NaAlSi}_3\text{O}_8$ has a light absorption coefficient of 0 near the visible wavelength

Fig. 9 The calculated (a) refractive index $n(\omega)$; (b) refractive index $k(\omega)$; (c) optical conductivity $\sigma_1(\omega)$; (d) optical conductivity $\sigma_2(\omega)$; (e) reflectivity $R(\omega)$; (f) loss function $L(\omega)$; and (g) absorption coefficient $I(\omega)$ of $\text{Al}_4[\text{Si}_4\text{O}_{10}](\text{OH})_8$



band. The absorption peak appears in the energy range of 15 eV, which is $2.9 \times 10^5 \text{ cm}^{-1}$. The main reason for the absorption peak is the electron transitions of the valence band electrons to the conduction band. The reflection coefficient is the proportion of the photon energy reflected from the surface to the photon energy striking the surface. When the energy is 20 eV, the reflectivity reaches the maximum value. The reflectivity in x , y , and z directions are 32.0%, 33.0%, and 35.2%, respectively. The loss function represents the energy loss of photoelectrons in

homogeneous media. The diagram shows a large number of dissipation peaks, which are highly relevant to plasma oscillations. Among them, the plasma frequencies L_n ($n = xx, yy, zz$) in three directions are 22.67, 22.63, and 22.78 eV, respectively.

As illustrated in Fig. 9, the refractive index of $\text{Al}_4[\text{Si}_4\text{O}_{10}](\text{OH})_8$ reaches a maximum value of 1.96 in the energy range of 10 eV. The trend of the extinction coefficient in the x , y direction is the same. In particular, the second peak of the extinction coefficient in the z direction is much larger than

other two directions, when the light utilization is improved. The absorption coefficient has two peaks, which achieve the maximum value of $3.2 \times 10^5 \text{ cm}^{-1}$ at the energy of 17 eV. When the energy is 21.6 eV, the reflectivity reaches the maximum value, and the reflectivity in the three directions of x , y , and z is 40.0%, 42.0%, and 45.8%, respectively. The calculated value of the plasma oscillation L_n ($n = xx, yy, zz$) are 21.13, 20.99, and 21.06 eV, respectively.

Conclusions

Overall, we calculated the structural, elastic, electronic, and optical properties of albite and kaolinite on the basis of first-principles calculations. The calculated lattice constants are consistent with the experimental data. The mechanical properties of $\text{NaAlSi}_3\text{O}_8$ and $\text{Al}_4[\text{Si}_4\text{O}_{10}](\text{OH})_8$ are studied. It shows that they have mechanical stability and brittleness. The energy band structure indicates that both of them are insulators with an indirect bandgap. By calculating the total density of states and the partial density of states, it can be seen that the main characteristics of the electronic structure of $\text{NaAlSi}_3\text{O}_8$ come from O-2p and Si-3p states, O-2p and Al-3p states hybridization, similar to $\text{Al}_4[\text{Si}_4\text{O}_{10}](\text{OH})_8$. For the purpose of investigating the bonding behavior of the materials, Mulliken charges, bond lengths, and bond populations were calculated for triclinic $\text{NaAlSi}_3\text{O}_8$ and $\text{Al}_4[\text{Si}_4\text{O}_{10}](\text{OH})_8$. The covalent property sequence of Si–O bands in $\text{NaAlSi}_3\text{O}_8$ is Si2-O3 > Si1-O4 > Si2-O2 > Si1-O8 > Si1-O6 > Si3-O2 > Si3-O4. The order of strength of the covalent bonding action in $\text{Al}_4[\text{Si}_4\text{O}_{10}](\text{OH})_8$ is Si1-O1 > Si1-O4 > Si1-O3 > Si1-O10 > Al1-O18 > Al1-O13 > Al1-O16 > Al1-O1 > Al1-O15 > Al1-O2. Optical anisotropy of triclinic $\text{NaAlSi}_3\text{O}_8$ and $\text{Al}_4[\text{Si}_4\text{O}_{10}](\text{OH})_8$ is observed.

Author contribution Ya-Le Tao: data curation, formal analysis, investigation, methodology, writing—original draft; Juan Gao: formal analysis, investigation, writing—review and editing; Qi-Jun Liu: conceptualization, investigation, methodology, project administration, supervision, writing—review and editing; Zheng-Tang Liu: methodology, software; all authors read and approved the final manuscript.

Funding This work was supported by the Sichuan Science and Technology Development Project (Grant No. 2021ZYD0027) and the Original Scientific Research Instrument and Equipment Development Project of Southwest Jiaotong University (Grant No. XJ2021KJZK055).

Data availability The data that support the findings of this study are available from the corresponding author upon reasonable request and available within the article.

Declarations

Competing interests The authors declare no competing interests.

Ethics approval Not applicable for both human and/or animal studies, we allow the journal to review all the data, and we confirm the validity of results. There is none of the financial relationships. This work was not published previously and it is not submitted to more than one journal. It is also not split up into several parts to submit. No data have been fabricated or manipulated.

Conflict of interest The authors declare no competing interests.

References

- Li B, Knowles KM (2013) *Modell Simul Mater Sci Eng* 21:055012
- Chen JH, Liu PS, Cheng W (2019) *Multidiscip Model Mater Struct* 15:659
- Sánchez-Soto PJ, Garzón E, Pérez-Villarejo L, Angelopoulos GN, Eliche-Quesada D (2021) *Minerals* 11:232
- Rouabhia F, Nemamcha A, Moumeni H (2018) *Cerâmica* 64:126
- Lerdprom W, Chinnam RK, Jayaseelan DD, Lee WE (2016) *J Eur Ceram Soc* 36:4319
- Pali M, Das S, Das SK (2015) *Bull Mater Sci* 38:551
- Gaudio SJ, Leshner CE, Maekawa H, Sen S (2015) *Geochim Cosmochim Acta* 157:28
- Siqueira RL, Peitl O, Zanotto ED (2016) *J Sol-Gel Sci Technol* 80:619
- Frizzo RG, Zaccaron A, Nandi VDS, Bernardin AM (2020) *Journal of Building Engineering* 31:101432
- Wang JY, Wang ZY, Yang LM, Yang GX, Miao CL, Lv PM (2017) *Energy* 141:1650
- Cao Z, Wang QZ, Cheng HF (2021) *Chin Chem Lett* 32:2617
- Alaba PA, Sani YM, Daud WMAW (2015) *RSC Adv* 5:11127
- Barbosa LV, Marcal L, Nassar EJ, Calefifi PS, Vicente MA, Trujillano R, Rives V, Gil A, Korili SA, Ciuffifi KJ, de Faria EH (2014) *Catalysis Today* 246:133
- Zhao J, Gao W, Qin XZ, He MC (2020) *Journal of the International Adsorption Society* 26:443
- Chen GB, Zhao HZ, Li X, Xia SW (2021) *Appl Clay Sci* 210:106120
- Sarma GK, Gupta SS, Bhattacharyya KG (2019) *SN Applied Sciences* 1:211
- Zhang B, Kang JT, Kang TH (2018) *Appl Surf Sci* 439:792
- Underwood T, Erastova V, Greenwell HC (2016) *J Phys Chem* 120:11433
- Xu HL, Jin XZ, Chen P, Shao G, Wang HL, Chen DL, Lu HX, Zhang R (2015) *Ceram Int* 41:6463
- Detellier C (2018) *Chem Rec* 18:868
- Kambel RD, Aliyu BA, Barminas JT, Akinterinwa A (2017) *International Journal of Materials and Chemistry* 7:14
- Liu TQ, Hu MY, Lu WT, Zhan JX, Cui XY, Zhan XH, Yu J (2019) *Physica B* 567:55
- Blasco M, Gimeno MJ, Auqué LF (2017) *Procedia Earth and Planetary Science* 17:120
- Sims M, Rucks M, Lobanov S, Young J, Daly JA, Pakhomova A, Konopkova Z, Liermann HP, Hrubciak R, Whitaker ML, Glotch TD, Ehm L (2019) *Lunar and Planetary Science Conference* 50:2132
- Li YH, Wang WZ, Huang SC, Wang K, Wu ZQ (2019) *Geochim Cosmochim Acta* 245:374
- Qin T, Wu F, Wu ZQ, Huang F (2016) *Contrib Mineral Petrol* 171:1
- Zhu C, Zhang YL, Rimstidt JD, Gong L, Burkhart JAC, Chen KY, Yuan HL (2021) *Geochim Cosmochim Acta* 303:15
- Xu LH, Peng TF, Tian J, Lu ZY, Hu YH, Sun W (2017) *Appl Surf Sci* 426:1005

29. Pietzsch A, Nisar J, Jämstorp E, Gråsjö J, Arhammar C, Ahuja R, Rubensson JE (2015) *J Electron Spectrosc Relat Phenom* 202:11
30. Shafei L, Adhikari P, Ching WY (2021) *Curr Comput-Aided Drug Des* 11:618
31. Weck PF, Kimb E, Jové-Colón CF (2015) *Dalton Trans* 44:12550
32. Yang H, He MC, Lu CS, Gong WL (2019) *Science China Physics, Mechanics & Astronomy* 62:1
33. Zhang ZJ, Zhou Q, Zhuang L, Zhao ZF (2021) *Mol Phys* 119:1896047
34. Wang J, Xia SW, Yu LM (2015) *Appl Surf Sci* 330:411
35. Aliatis I, Lambruschi E, Mantovani L, Bersani D, Andò S, Gatta GD, Gentile P, Salvioli-Mariani E, Prencipe M, Tribaudino M, Lottici PP (2015) *J Raman Spectrosc* 46:501
36. Cano NF, Santos LHED, Chubaci JFD, Watanabe S (2015) *Spectrochim Acta Part A Mol Biomol Spectrosc* 137:471
37. Amulele GM, Lanati AW, Clark SM (2022) *Am Miner* 107:614
38. Brown JM, Angel RJ, Ross NL (2016) *Journal of Geophysical Research: Solid Earth* 121:663
39. Lacivita V, D'Arco P, Mustapha S, Bernardes DF, Dovesi R, Erba A, Rérat M (2020) *Physics and Chemistry of Minerals* 47:45
40. Liu XX, Liu XW, Hu YH (2015) *Clay Miner* 50:199
41. Zhu HW, Xiao XY, Guo ZH, Han XQ, Liang YQ, Zhang Y, Zhou C (2018) *Appl Clay Sci* 161:310
42. Clark SJ, Segall MD, Pickard CJ, Hasnip PJ, Probert MIJ, Refson K, Payne MC (2005) *Z Kristallogr* 220:567
43. Perdew JP, Zunger A (1981) *Phys Rev B* 23:5048
44. Monkhorst HJ, Pack JD (1976) *Phys Rev B* 13:5188
45. Winter JK, Ghose S, Okamura FP (1977) *Am Miner* 62:921
46. Young RA, Hewat AW (1988) *Clays Clay Miner* 36:225
47. Yu ED, Pan Y (2022) *Journal of Materials Chemistry A* 46:24866
48. Yu ED, Pan Y (2022) *Electrochim Acta* 435:141391
49. Chen S, Pan Y (2022) *Appl Surf Sci* 599:154041
50. Pan Y, Yu ED (2022) *Int J Hydrogen Energy* 47:27608
51. Pan Y (2023) *J Phys Chem Solids* 174:111152
52. Liu WH, Liu QJ, Zhong M, Gan YD, Liu FS, Li XH, Tang B (2022) *Acta Mater* 236:118137
53. Born M (1940) *Math Proc Cambridge Philos Soc* 36:160
54. Gao J, Liu QJ, Jiang CL, Fan DH, Zhang M, Liu FS, Tang B (2022) *Chinese Journal of High Pressure Physics* 36:051101
55. Chung DH, Buessem WR (1967) *J Appl Phys* 38:2010
56. Pugh SF (1954) *The London, Edinburgh, and Dublin Philosophical Magazine and Journal of Science* 45:823
57. Gao J, Zeng W, Tang B, Zhong M, Liu QJ (2021) *Mater Sci Semicond Process* 121:105447
58. Horsley SAR, Artoni M, Rocca GCL (2015) *Nat Photonics* 9:436
59. Zhong M, Zeng W, Liu FS, Fan DH, Tang B, Liu QJ (2022) *Mater Today Phys* 22:100583
60. Ambrosch-Draxl C, Sofo JO (2006) *Comput Phys Commun* 175:1

Publisher's Note Springer Nature remains neutral with regard to jurisdictional claims in published maps and institutional affiliations.

Springer Nature or its licensor (e.g. a society or other partner) holds exclusive rights to this article under a publishing agreement with the author(s) or other rightsholder(s); author self-archiving of the accepted manuscript version of this article is solely governed by the terms of such publishing agreement and applicable law.